また、ネガマイシン群について、今回の成果は合成研究を経て既存薬とは構造的に全く異なる遺伝子疾患治療薬創製を可能にしたと考える。

G. 研究発表

1. 論文発表

T. Watanabe, I. Momose, M. Abe, H. Abe, R. Sawa, Y. Umezawa, D. Ikeda, Y. Takahashi & Y. Akamatsu. Synthesis of boronic acid derivatives of tyropeptin: Proteasome inhibitors. Bioorg. Med. Chem. Lett. 19: 2343-2345 (2009)

T. Ito, N. Abe, Y. Masuda, M. Nasu, M. Oyama, R. Sawa, Y. Takahashi & M. Iinuma. Two Novel Resveratrol Derivatives from the Leaves of Vateria indica. Helv. Chem. Acta. 92: 195-208 (2009)

I. Miyazaki, H. Okumura, S. Simizu, Y. Takahashi, N. Kanoh, Y. Muraoka, Y. Nonomura & H. Osada. Structure-Affinity Relationship Study of Bleomycins and Shble Protein by Use of a Chemical Array. Chembiochem. 10: 845-852 (2009)

Shiozuka M, Wagatsuma A, Kawamoto T, Sasaki H, Shimada K, Takahashi Y, Nonomura Y, and Matsuda R. Transdermal delivery of a readthrough-inducing drug: a new approach of gentamicin administration for the treatment of nonsense mutation-mediated disorders. J. Biochem. 147: 463-470 (2010)

2. 学会発表

阿部尚仁，伊藤哲朗，大山雅義，澤　竜一，高橋良和，飯沼宗和　フタバガキ科植物Vatica albiramisのスチルベンオリゴマーの構造　第５１回天然有機化合物討論会

藤巻貴宏，河村達郎，高橋良和，五十嵐雅之，木下直子，西村吉雄，田代　悦，井本正哉　微生物由来新規アンドロゲンアンタゴニストHE21の発見　日本農芸化学会2010年度

渡辺　匠，梅沢洋二，高橋良和，赤松　穣　ヴァーチャルスクリーニングによるオキシドスクアレン環化酵素阻害剤の探索　日本薬学会第130回年会

田口晃弘，伊奈真友子，野本貴雄，山崎有理，薬師寺文華，高橋良和，野々村禎昭，林　良雄　ヒドラジンアミド部位に着目したネガマイシン誘導体の合成

研究成果の刊行に関する一覧表

雑誌

Shiozuka M, Wagatsuma A, Kawamoto T, Sasaki H, Shimada K, Takahashi Y, Nonomura Y, and Matsuda R. Transdermal delivery of a readthrough-inducing drug: a new approach of gentamicin administration for the treatment of non-sense mutation-mediated disorders. J. Biochem. 147: 463-470 (2010)

Kikkawa N, Ohno T, Nagata Y, Shiozuka M, Kogure T, and Matsuda R. Ectopic calcification is caused by elevated levels of serum inorganic phosphate in mdx mice. Cell Struc. Func., 34: 77-88 (2009)

塩塚政孝，我妻玲，松田良一，筋ジストロフィーの薬物治療 –リードスルー薬物による挑戦–，小児科診療 72: 763 (2009)

## 研究成果による特許権等の知的財産権の出願状況

「ナンセンス変異型疾患の治療方法」　PCT出願（PCT/JP2007/063436）

「リードスルー誘導剤，及びナンセンス変異型遺伝性疾患治療薬」特願2010-021817

J. Biochem. 2010;147(4):463–470 doi:10.1093/jb/mvp185

JB THE JOURNAL OF BIOCHEMISTRY

# Transdermal delivery of a readthrough-inducing drug: a new approach of gentamicin administration for the treatment of nonsense mutation-mediated disorders

*Received July 13, 2009; accepted November 4, 2009; published online November 11, 2009*

**Masataka Shiozuka[1], Akira Wagatsuma[1], Tadafumi Kawamoto[2], Hiroyuki Sasaki[3], Kenichi Shimada[1], Yoshikazu Takahashi[4], Yoshiaki Nonomura[4] and Ryoichi Matsuda[1,*]**

[1]Department of Life Sciences, Graduate school of Arts and Sciences, The University of Tokyo, 3-8-1 Komaba, Meguro-ku, Tokyo 153-8902; [2]Radioisotope Research Institute, Tsurumi University, Yokohama 230-8501; [3]Institute of DNA Medicine, The Jikei University School of Medicine, Tokyo 105-8461; and [4]Microbial Chemistry Research Foundation, Tokyo 141-0021, Japan

*Ryoichi Matsuda, Department of Life Sciences, Graduate school of Arts and Sciences, The University of Tokyo, 3-8-1 Komaba, Meguro-ku, Tokyo 153-8902, Japan. Tel.: +81-3-5454-6637; Fax: +81-3-5454-4306; E-mail: cmatsuda@mail.ecc.u-tokyo.ac.jp

**To induce the readthrough of premature termination codons, aminoglycoside antibiotics such as gentamicin have attracted interest as potential therapeutic agents for diseases caused by nonsense mutations. The transdermal delivery of gentamicin is considered unfeasible because of its low permeability through the dermis. However, if the skin permeability of gentamicin could be improved, it would allow topical application without the need for systemic delivery. In this report, we demonstrated that the skin permeability of gentamicin increased with the use of a thioglycolate-based depilatory agent. After transdermal administration, the readthrough activity in skeletal muscle, as determined using a *lacZ/luc* reporter system, was found to be equivalent to systemic administration when measured in transgenic mice. Transdermally applied gentamicin was detected by liquid chromatography-tandem mass spectrometry in the muscles and sera of mice only after depilatory agent-treatment. In addition, expansion of the intercellular gaps in the basal and prickle-cell layers was observed by electron microscopy only in the depilatory agent-treated mice. Depilatory agent-treatment may be useful for the topical delivery of readthough-inducing drugs for the rescue of nonsense mutation-mediated genetic disorders. This finding may also be applicable for the transdermal delivery of other pharmacologically active molecules.**

*Keywords*: Gentamicin/nonsense mutation/readthrough/thioglycolates/transdermal drug delivery.

*Abbreviations*: TEM, transmission electron microscopy; TCA, trichloroacetic acid.

More than 1800 distinctly inherited human diseases are caused by a single gene that carries nonsense mutations (*1*). In *Duchenne* muscular dystrophy (DMD), up to 20% of patients carry nonsense mutations (*2*). Similarly, up to 10% of patients (>50% in Israel) with cystic fibrosis (CF) have nonsense mutations in the CF transmembrane regulator gene (*3*). Nonsense mutations in tumour-suppressor genes are also common during the development and progression of cancer (*4*). Despite advances in gene therapy, clinical success is pending. One limitation involves the inducing genes used in the therapy, which are often targeted by the patient's autoimmune system in response to the viral proteins encoded in the vector. An alternative, pharmacologic approach to induce translational readthrough involves blocking the nonsense mutations using antibiotics. It has been reported that aminoglycoside antibiotics can interfere with the fidelity of the translation machinery. Aminoglycosides cause extensive miscoding of the mRNA *in vitro* (*5*) and allow readthrough of premature termination codons, as demonstrated in *Escherichia coli* (*6*), tetrahymena (*7*), wheat embryos (*8*), yeast (*9*), cultured mouse cells (*10*) and human cells (*11–14*).

The *mdx* mouse, which is a naturally occurring animal model for DMD, carries a point mutation (from CAA to TAA) at position 3185 in exon 23 of the dystrophin gene. Barton-Davis *et al.* (1999) reported that gentamicin restored functional dystrophin in the *mdx* mouse (*15*). Moreover, clinical trials involving patients with DMD or CF caused by nonsense mutations have shown that aminoglycosides suppress premature termination mutations in some cases (*16*, *17*).

Gentamicin is one of the most commonly used aminoglycoside antibiotics, and it is usually administered by intramuscular injection. However, it cannot be administered either orally or transdermally as it is a polarized water-soluble compound with very poor intestinal and dermal permeability. Less painful and simpler methods of gentamicin administration are needed to improve the care of patients with genetic disorders caused by nonsense mutations. To this end, transdermal drug delivery has several advantages: it: (i) bypasses gastrointestinal incompatibility and the hepatic 'first-pass' effect; (ii) reduces side-effects due to the optimization of the blood concentration-time profile; (iii) involves patient-activated/patient-modulated delivery which enhances patient compliance; and (iv) enhances target specificity (*18*). However, a major limitation of transdermal administration is the difficulty associated with delivering gentamicin through the skin barrier.

The objective of the present study was to evaluate the *in vivo*, chemically enhanced transdermal delivery of gentamicin as a readthrough-inducing drug. To this end, we established a novel transgenic mouse strain, named READ (Readthrough Evaluation and Assessment by Dual-reporter), that carries a dual-reporter gene composed of the *lacZ* and *luc* genes connected with a premature termination codon. In this system, only β-galactosidase can be translated without transcriptional readthrough, however, both enzymes would be translated when readthrough occurs. In addition, liquid chromatography-tandem mass spectrometry (LC-MS/MS) was used to validate the effect of a depilatory agent on the *in vivo* permeation of gentamicin. Finally, ultrastructural studies using electron microscopy were performed to provide insight into the potential mechanism of barrier alterations in depilatory agent-treated skin.

## Materials and Methods

### Chemicals

Gentamicin solution (Gentacin injection) and cream (0.1% Gentacin cream) were purchased from Schering-Plough K. K. (Osaka, Japan). Hair removal gel mousse was obtained from Reckitt Benckiser Co., Ltd. (Tokyo, Japan). All other chemicals were purchased from Sigma Chemical Co. (St Louis, MO, USA), Wako Pure Chemical Industries (Osaka, Japan) and Promega (Madison, WI, USA).

### Animals

A dual-reporter transgenic mouse strain on a C57/BL6 background was generated by the Bioindustry Division of Oriental Yeast Co., Ltd (Tokyo, Japan). The dual-reporter gene consisted of the genes encoding β-galactosidase and luciferase connected with the premature termination codon 'Opal (TGA)' region (a 27-mer that contains the sequence surrounding the premature termination codon of exon 23 of the *mdx* gene for mouse dystrophin; TTGAAAGAG CAATAAAATGGCTTCAAC), and was driven by a cytomegalovirus/β-actin hybrid promoter (Fig. 1). Transgene DNA was injected into the male pronuclei of fertilized eggs which were then incubated at 37°C and transferred into the uteri of pseudopregnant ICR recipient female mice. Founder mice bearing the transgene were identified by PCR analysis of the DNA isolated from partially excised tails. Homozygous transgenic mice were obtained after crossing heterozygous littermates.

Male hairless (HR1) and normal (C57/BL6) mice (5 weeks old; ~25 g body weight) were obtained from Japan SLC, Inc. The mice were housed individually under controlled conditions of temperature and humidity and had free access to water and food. The mice were procured after approval for the present study from the University of Tokyo Animal Ethics Committee.

### Skin treatment and readthrough analysis

A thioglycolate-based depilatory cream was applied for 1 min to the mouse skin, which was then rinsed with warm water to remove the cream. Gentamicin cream (1 mg gentamicin/day) was then applied and rubbed gently onto the skin daily for 7 days. At the completion of the treatment, the mice were euthanized with an overdose of ether. Tissue samples were collected from the latissimus dorsi, gluteus major, femoris lateralis, biceps femoris and quadriceps femoris. Dissected tissues were minced with scissors and homogenized in three volumes of the reporter lysis buffer (Promega) with thin glass fragments using a tissue grinder (Physcotron, Niti-on, Japan). Tissue homogenates were subjected to one round of freeze-thawing. For the readthrough assay, the lysate supernatants were collected after centrifugation at 17710*g* for 10 min, and then analyzed using the Beta-Glo and Bright-Glo luciferase assay systems (Promega).

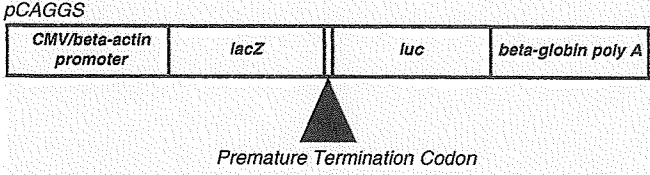


**Fig. 1 Schematic structure of the dual-reporter gene construct.** The dual reporter was composed of the *lacZ* and *luc* genes connected with a premature termination codon region derived from exon 23 of the *mdx* mouse dystrophin gene and driven by a cytomegalovirus/β-actin hybrid promoter. Although the premature termination codon was originally TAA, we used TGA in the present study.

The β-galactosidase and luciferase activities were measured according to the manufacturers' instructions using a luminometer (Luminescencer-JNRII, AB-2300; Atto, Japan). The readthrough efficiency was determined as the ratio of luciferase activity to β-galactosidase activity.

### Liquid chromatography-tandem mass spectrometry

To trace the gentamicin introduced into the mice, LC-MS/MS analysis was performed using the 1100 Quaternary HPLC System (Agilent Technologies, USA) coupled to the API 5000 (Applied Biosystems, CA, USA). Gentamicin solution (10 ng/ml in 5% TCA), 5% TCA and blank mouse serum or muscle tissue extract in reporter lysis buffer were added in equal quantities to serve as the gentamicin standard samples. To prepare the samples for LC-MS/MS, the supernatant of the serum or muscle tissue extract was mixed with 5% TCA (twice the volume of the sample). Chromatographic separation was performed on an XTerra column (3.5 μm, 2.1 mm × 50 mm, Waters, MA, USA) maintained at 30°C in a column oven. Five millimolar hepatafluorobutyric acid (solvent A) and acetonitrile (solvent B) were used as the mobile phase under the condition of 10% B (0–2 min), 10–30% B (2–4 min, linear gradient), 30% B (4–10 min), 10–30% B (10–12 min, linear gradient), and 10% B (12–15 min) at a flow rate of 0.2 ml/min with an injection volume of 10 μl. The parent to product ion transitions for gentamicin (*m/z* 478.39→322.30 as gentamicin C1) was monitored on a triple quadrupe mass spectrometer, operating in the multiple reaction monitoring (MRM) with a positive ion mode of electrospray ionization (ESI) and a data collection time of 15 min. The relative quantitative value was calculated using the single-level, calibration-curve method.

### Histochemical and electron microscopic analyses

Serial fresh-frozen sections (10 μm thickness) from the whole body of a mouse were prepared according to Kawamoto's film method (*19*). The whole-body sections were freeze-dried and then incubated in X-Gal solution (Nakarai, Japan) overnight at 37°C, and then placed in PBS. The adjacent sections were stained with Hematoxylin and Eosin.

For TEM analysis, small pieces (10 mm × 10 mm) of the dorsal side of the skin were excised from the hairless mice with a single-edge razor blade. To prepare ultra-thin sections for electron microscopy, tissues were doubly fixed with 2% glutaraldehyde in 0.1 M phosphate buffer and 1% osmium tetroxide (in 0.1 M phosphate buffer), and then dehydrated with a graded series of ethanol. The tissues were then embedded in epoxy resin. Ultra-thin sections were stained with uranyl acetate and lead citrate and observed under an electron microscope (H-7500; Hitachi, Tokyo, Japan) at an acceleration voltage of 100 kV. The images were optimized for contrast and brightness using Photoshop CS3 software (Adobe Inc., San Jose, USA).

## Results

### Establishment of a transgenic mouse for transcriptional readthrough evaluation

In order to measure transcriptional readthrough activity, we established a novel transgenic mouse strain, named READ, which expressed a dual-reporter gene. The dual reporter construct was composed of the *lacZ* and *luc* genes connected with a premature termination codon region (Fig. 1). Although the premature termination codon of the *mdx* mouse was originally TAA, we adopted TGA-centered sequences because

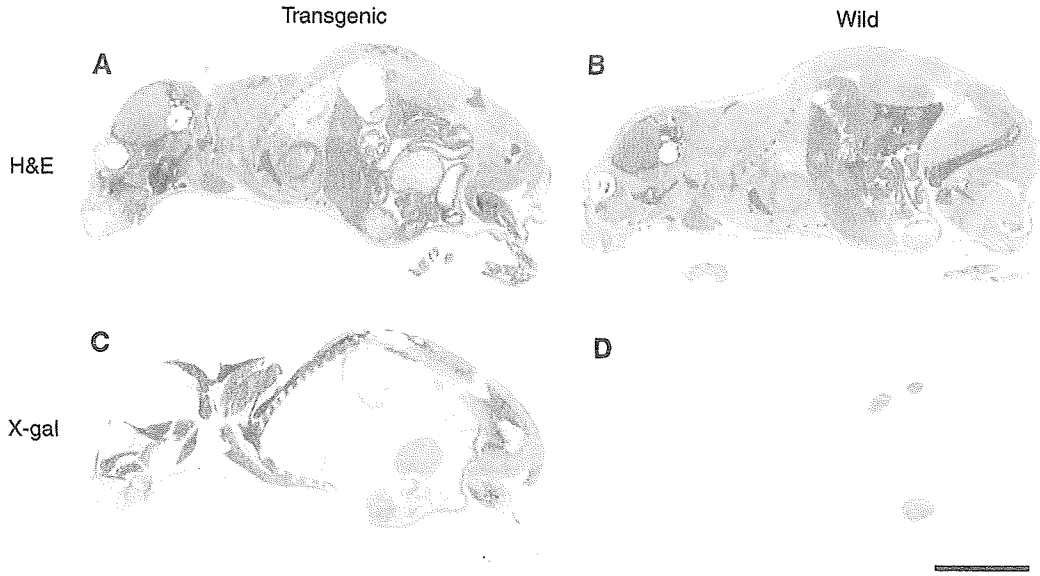


**Fig. 2 Whole-body X-gal staining of a transgenic mouse.** Whole-body fresh sections of 5-week-old transgenic (A and C) and control (B and D) mice were stained with Hematoxylin-Eosin (A and B) and X-gal (C and D). The transgenic mouse expressed β-galactosidase in the skeletal and cardiac muscles. The contents of the digestive tracts stained positive with X-gal due to the native bacterial β-galactosidase of flora (D). Bar = 1 cm.

aminoglycoside antibiotics tend to exhibit the highest readthrough activity for TGA (*20*). When a test substance without readthrough activity was administered to READ mice, only β-galactosidase was translated. We confirmed β-galactosidase expression in striated muscles, including the diaphragm and heart, by X-gal staining of whole-body sections (Fig. 2C). The readthrough efficiency was determined as the ratio of luciferase activity to β-galactosidase activity.

### *Readthrough activity of gentamicin in READ mice*

The readthrough activities of gentamicin following single, daily subcutaneous injections (1 mg in 0.1 ml, $n=6$) and transdermal administration (1 mg in 1 g, $n=5$) after depilatory treatment were compared after 7 days. The mice used for transdermal administration were treated with depilatory cream on day zero. A commercially available topical cream containing 0.1% gentamicin was then applied daily to the skin of the back, hip and thigh of each transgenic mouse. Gentamicin applied to the depilatory agent-treated skin induced readthrough in the muscle tissues at the same level as that observed after subcutaneous injection (Fig. 3). Transdermally administered gentamicin resulted in readthrough activity only in depilatory agent-treated READ mice, but not in untreated ones.

### *Detection of gentamicin in muscle and serum of subcutaneously and transdermally treated mice*

To study the permeability of gentamicin into the muscle tissues, LC-MS/MS analysis was performed. The presence of gentamicin C1 was confirmed in both the subcutaneously and transdermally treated groups (Fig. 4). The gentamicin components C1a and C2 were also detected in the same manner (data not shown). To evaluate whether pretreatment with the thioglycolate-based depilatory agent enhances gentamicin permeation through the skin, the detection of

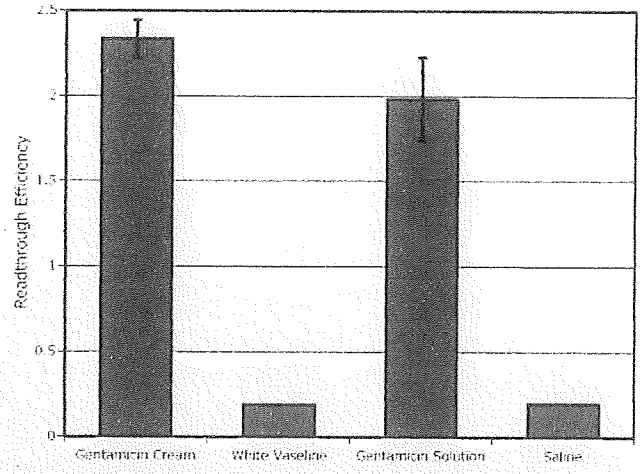


**Fig. 3 Effects of topical and subcutaneous administration of gentamicin on readthrough activity in READ mice.** The readthrough activity of gentamicin was compared between mice that were treated by daily topical administration (1 mg in 1 g, $n=5$) onto depilatory-treated skin and those treated by subcutaneous injection (1 mg in 100 µl, $n=6$) for 7 days. The data for gentamicin cream administration showed the same increase in readthrough efficiency as that observed for subcutaneous injection (gentamicin solution). Error bars indicate SDs.

gentamicin in the sera and muscle tissue extracts of hairless mice was carried out using LC-MS/MS. We confirmed that the LC-MS/MS peak observed for the depilatory-treated group was in the identical position as that of the reference material, whereas the peak associated with gentamicin C1 was undetectable in the untreated group (Fig. 5). The results indicate that the depilatory agent significantly increased the absorption of gentamicin by the skin.

### *Ultrastructure of depilatory agent-treated skin*

To examine whether ultrastructural changes in the skin were caused by treatment with the depilatory agent,

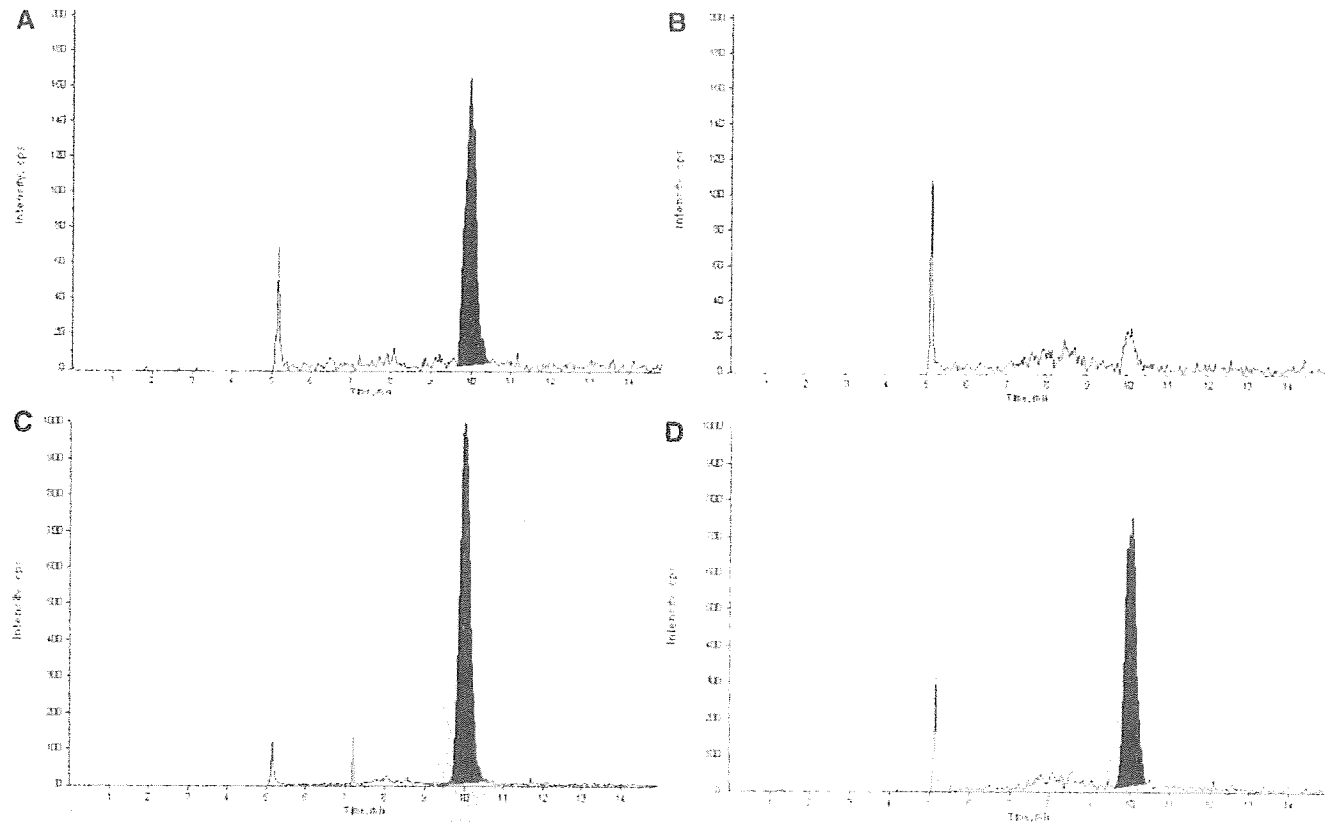


**Fig. 4 LC-MS/MS detection of gentamicin in the muscle tissue extracts from gentamicin-treated mice.** The mass chromatograms of gentamicin C1 in muscle tissue extracts from C57/BL6 mice: gentamicin standard sample (A); no administration (B); subcutaneous injection of gentamicin daily for 7 days (C); transdermal administration of gentamicin cream daily for 7 days after one-time depilatory treatment (D). The major (black-painted) peak obtained for both administration groups was identical to the gentamicin standard sample.

TEM analysis was performed with control, 1 min- and 24 h-treated samples. In the non-treated control sample, the cells were closely packed together and intercellular spaces were not observed (Fig. 6A). However, even after just 1 min of treatment with the depilatory agent, the formation of gaps could be observed when the control (Fig. 6A) and experimental sample (Fig. 6B) were compared. In the sample treated 24 h with the depilatory agent, a large expansion of the intercellular gaps and extraordinary spaces in the basal and prickle-cell layers were clearly evident (Fig. 6C).

## Discussion

### *Establishment of a transgenic mouse for the in vivo assay of readthrough activity*

We established and demonstrated the efficacy of a dual-reporter transgenic mouse strain, named READ, which can be used for the detection of readthrough activity *in vivo* for the first time. It is difficult to measure the amount of dystrophin quantitatively because it is relatively large (molecular weight of 427 kDa) and is only present in small amounts in striated muscles. Therefore, the reporter assay with READ mouse is quantitative and efficient in comparison to the detection of dystrophin using a *mdx* mouse. In rare cases, some luciferase inhibitors, a compound such as PTC124, acting through post-translational *luc* reporter stabilization, appear to activate gene expression (*21*). We consider the importance of implementing the appropriate control assays. The READ mouse assay system used in this study makes it possible not only to screen new molecules which induce readthrough, but also to examine the pharmacokinetics and side effects associated with such molecules. This system can also be used for the optimization of various routes of drug administration. Our READ mouse provides a powerful and valuable tool for the development of novel readthrough therapeutics.

### *Depilatory agent-treatment enhances dermal permeability and is useful for transdermal drug delivery*

Transdermal drug delivery systems offer many advantages over conventional dosage forms, such as improved patient compliance, reduced side effects, no hepatic first pass effects, and the possibility to easily interrupt or terminate treatment (*22–24*). Moreover, compared with oral administration, such a non-invasive drug delivery route significantly reduces drug degradation due to the lower metabolic activity at the site of administration. It also bypasses hepatic circulation which is a major site of potential drug metabolism (*25*). However, given the low permeability of external molecules, such as gentamicin, the skin remains a minor portal of entry for drugs (*26*). Therefore, various approaches aimed at decreasing the resistance of skin to drug penetration have been investigated (*27*). The effects of a depilatory agent on the percutaneous absorption of testosterone and theophylline in Guinea pigs (*28*) and rats (*29*), respectively, and on the

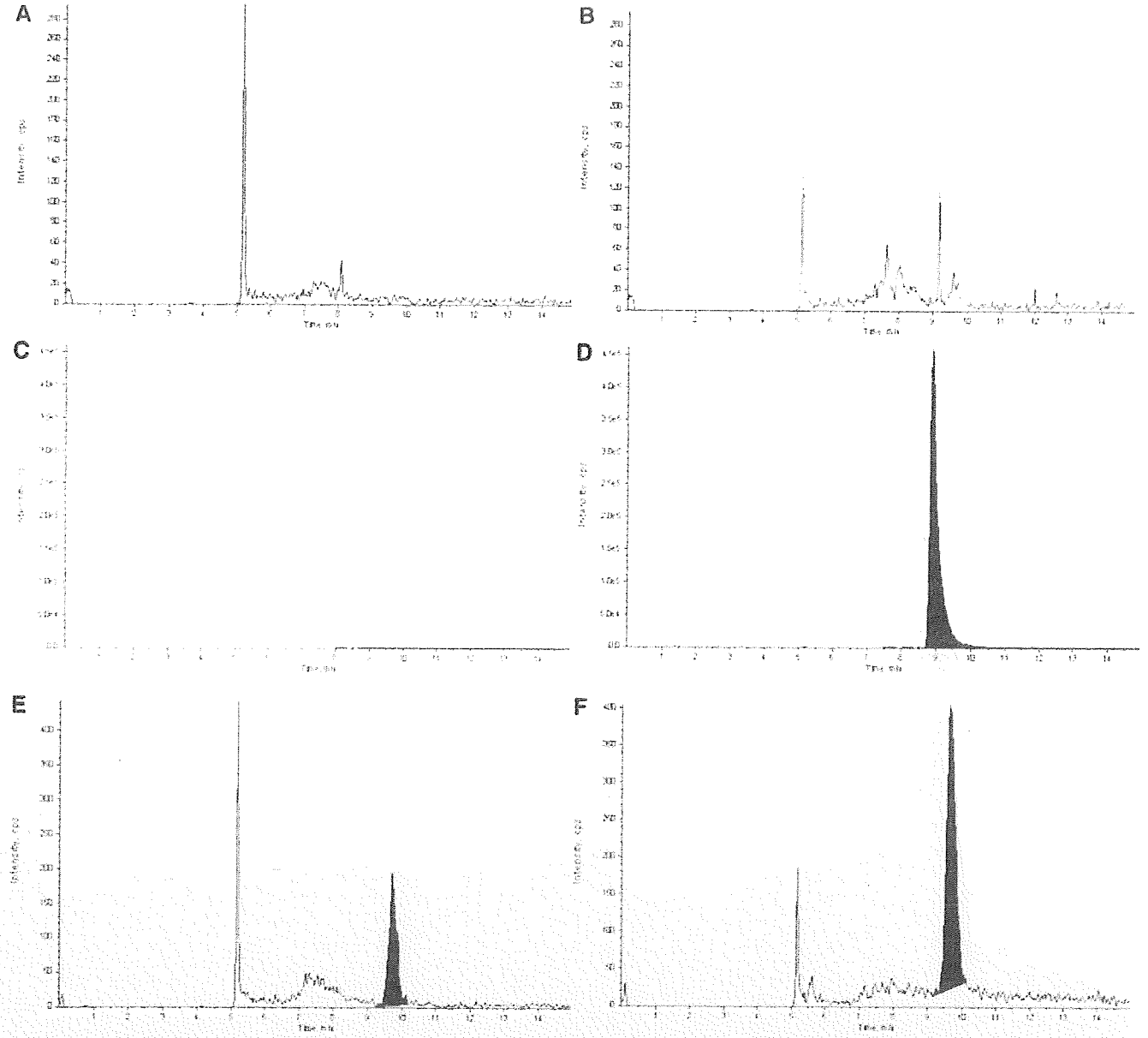


**Fig. 5 LC-MS/MS detection of gentamicin in the sera and muscle tissue extracts of hairless mice with or without depilatory treatment.** Mass chromatograms of gentamicin C1 in the sera (A, C and E) and muscle tissue extracts (B, D and F) from hairless mice: non-depilatory-treated and gentamicin-administrated daily for 7 days (A and B); one-time depilatory-treated 24 h prior to administration and gentamicin-administrated daily for 7 days (C and D); part of (C) at a higher magnification (E); gentamicin standard sample (F). The black-painted peak showed the existence of gentamicin. Gentamicin was not detected in the non-depilatory-treated group, whereas gentamicin was present in the depilatory-treated-group, as assessed by comparison with the reference material in LC-MS/MS.

ionotophoretic delivery of insulin in diabetic rats (*30*, *31*), porcine epidermis (*32*, *33*), and on the human stratum corneum (*34*) have been reported. As shown in Fig. 3, topically applied gentamicin cream induced the readthrough of a premature termination codon and was as effective as subcutaneous injection.

### *Presence of transdermally delivered gentamicin in muscle and serum*

To determine whether a depilatory agent could influence the permeability of skin, we next investigated the permeation of gentamicin following transdermal administration using a validated LC-MS/MS system (Fig. 4). The quantity of gentamicin was calculated from the peak area and when appropriate, we normalized the measured levels to a peak area of known concentration in a gentamicin standard sample. In the muscle tissue extracts, the concentration of gentamicin was ~2-fold higher on average ($n = 3$) for transdermal administration when compared to subcutaneous injections. It is likely that transdermal administration can extend the duration of treatment with gentamicin, which has a short half-life.

The administered gentamicin was present in both the sera and muscle tissue extracts of depilatory agent-treated mice (Fig. 5). Furthermore, LC-MS/MS results indicated that the amount of gentamicin was significantly higher (~7000-fold) in the muscle tissue than in the serum. *In vivo* transdermal absorption experiments demonstrated that the depilatory agent drastically reduced the barrier function of the skin

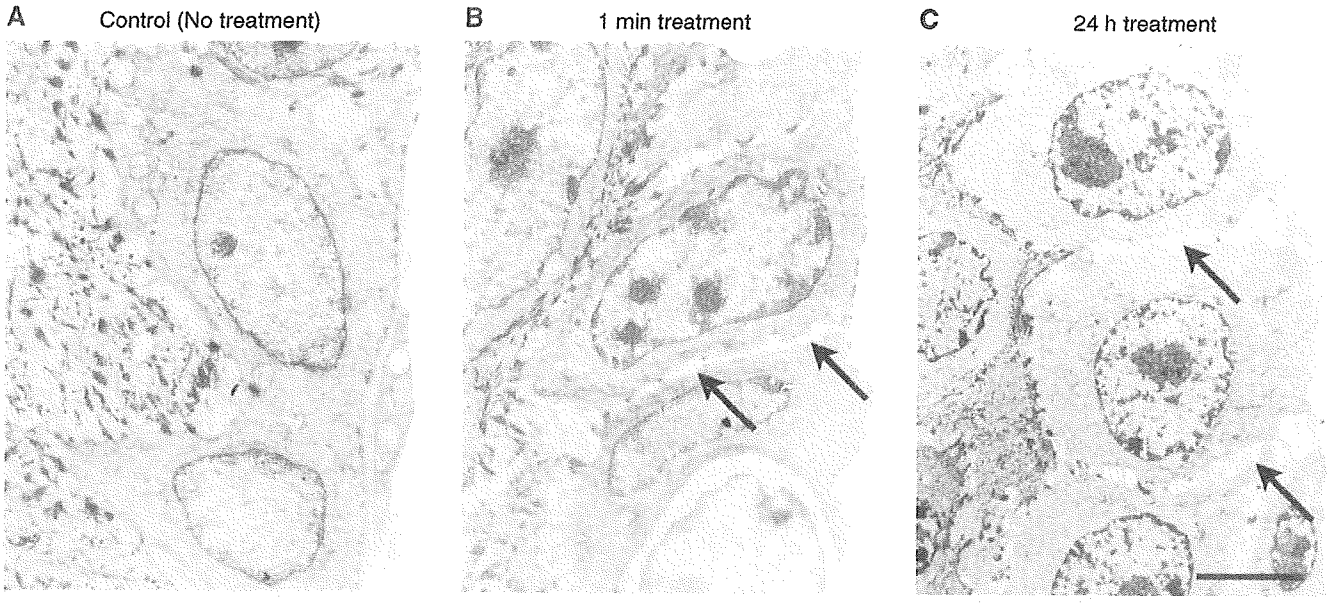


**Fig. 6 Electron micrographs of skin samples from hairless mice treated with a depilatory cream.** Dorsal skin samples from 5-week-old hairless mice; control (non-depilatory-treated) (A); treated with the depilatory cream for 1min (B); and treated with depilatory cream for 24 h during the study (C). Expansion of the intercellular gaps in the basal and prickle-cell layers caused by depilatory processing was evident (B and C, arrows). Bar = 5 μm.

and exerted a direct penetration-enhancing effect on the transdermal route. However, these may be based on the difference in hairless mouse and normal hairy mouse. The hairless mice have been widely and frequently used to predict the effects of penetration enhancers in human skin. Nevertheless, the information on the suitability of hairless mice in percutaneous penetration is not uniform and sometimes contradictory (*35*). The skin of hairless mice is obviously thin in comparison with normal mice and has many folds. Moreover, because the skin penetration is a complex process, a judgement about this penetration-enhancing effect on hairless mouse skin must be cautious. In addition, we can conclude that differences in the delivery vehicles affect the penetration and bioavailability of the drug. Specifically, the effectiveness of gentamicin in an emulsion base (i.e. a cream) was higher than in oils and fats as determined by the readthrough activity and the LC-MS/MS analysis (data not shown).

### *Depilatory agent-treatment causes ultrastructural changes in the skin*

To gain further insight into the mechanisms by which depilatory agents affect skin permeability, we evaluated ultrastructural changes in the skin caused by a thioglycolate-based depilatory agent (Fig. 6). As compared to the non-treated control, both the 1 min- and 24 h-treatments disrupted the structural integrity of the basal and prickle-cell layers. Jin-Ning Lee and colleagues (*34*) have shown that depilatory agents enhance transepidermal drug delivery by reducing the resistance of both the transcellular and intercellular routes of the stratum corneum. Our present results indicate that the alteration and expansion of the intracellular spaces in the basal and prickle-cell layers could be due to the shrinkage of cells in those layers, which in turn leads to reduced resistance.

### *Readthrough for rescuing muscular dystrophy*

In this study, we selected gentamicin to evaluate the efficacy of topical drug delivery. Aminoglycosides have emerged as vanguard pharmacogenetic agents for the treatment of human genetic disorders due to their ability to suppress translation termination caused by nonsense mutations. Gentamicin injections into *mdx* mice, a model for DMD, restored dystrophin in up to 20% of the muscle fibres and ameliorated the clinical symptoms of diseases (*15*). As gentamicin can cause serious side effects, such as inner ear and kidney toxicities, and may generate resistant bacteria, non-aminoglycoside, readthrough-inducing molecules are being actively sought. Previously, we reported that the dipeptide antibiotic negamycin has the ability to suppress nonsense mutations with lower toxicity than gentamicin (*36–38*). Thus, negamycin and its derivatives represent therapeutic candidates for genetic disorders, and are a topic for future studies. The small-molecular agent PTC124 (also known as Ataluren) has also been reported as a promising readthrough drug for DMD patients with nonsense mutations (*39*). Our transgenic mouse would be applicable to investigate the potential *in vivo* readthrough activity of these and other new molecules.

In the present study, we demonstrated that a transdermally delivered readthrough drug promotes the bypassing of a premature termination codon, which represents a novel approach for the treatment of genetic diseases caused by nonsense mutations. The transdermal delivery of drugs involves the continuous administration of therapeutic molecules through the skin, and has many advantages including the maintenance of low plasma drug levels and improving patient

compliance. We also showed the effectiveness of a thioglycolate-based depilatory agent to enhance the topical delivery of gentamicin. This finding may also be applicable for the transdermal delivery of other pharmacologically active molecules.

## Acknowledgements

The authors would like to thank Dr Ryuichi Sawa for his helpful advice regarding the LC-MS/MS method.

### Funding

Health and Labour Sciences Research Grant [19A-020] for Research on Psychiatric and Neurological Diseases and Mental Health, and a Research Grant for Nervous and Mental Disorders [20B-13] from the Ministry of Health, Labour and Welfare, Japan.

### Conflict of interest

None declared.

## References

1. Kellermayer, R. (2006) Translational readthrough induction of pathogenic nonsense mutations. *Eur. J. Med. Genet.* **49**, 445–450
2. Diop, D., Chauvin, C., and Jean-Jean, O. (2007) Aminoglycosides and other factors promoting stop codon readthrough in human cells. *C. R. Biol.* **330**, 71–79
3. Kerem, E., Hirawat, S., Armoni, S., Yaakov, Y., Shoseyov, D., Cohen, M., Nissim-Rafinia, M., Blau, H., Rivlin, J., Aviram, M., Elfring, G., Northcutt, V., Miller, L., Kerem, B., and Wilschanski, M. (2008) Effectiveness of PTC124 treatment of cystic fibrosis caused by nonsense mutations: a prospect phase II trial. *Lancet* **372**, 719–727
4. Kaufman, R. (1999) Correction of genetic disease by making sense from nonsense. *J. Clin. Invest.* **104**, 367–368
5. Davies, J., Gorini, L., and Davis, B.D. (1965) Misreading of RNA codewords induced by aminoglycoside antibiotics. *Mol. Pharmacol.* **1**, 93–106
6. Gorini, L. (1974) Ribosomes (Nomura, M., Tissieres, T., and Lengyel, P., eds), pp. 791–803, Cold Spring Harbor Laboratory Press, NY
7. Palmer, E. and Wilhelm, J.M. (1978) Mistranslation in a eukaryotic organism. *Cell* **13**, 329–334
8. Wilhelm, J.M., Jessop, J.J., and Pettitt, S.E. (1978) Aminoglycoside antibiotics and eukaryotic protein synthesis: stimulation of errors in the translation of natural messengers in extracts of cultured human cells. *Biochemistry* **17**, 1149–1153
9. Palmer, E., Wilhelm, J.M., and Sherman, F. (1979) Phenotypic suppression of nonsense mutants in yeast by aminoglycoside antibiotics. *Nature* **277**, 148–150
10. Sangkuhl, K., Schulz, A., Rompler, H., Yun, J., Wess, J., and Schoneberg, T. (2004) Aminoglycoside-mediated rescue of a disease-causing nonsense mutation in the V2 vasopressin receptor gene *in vitro* and *in vivo*. *Hum. Mol. Genet.* **13**, 893–903
11. Wilhelm, J.M., Jessop, J.J., and Pettitt, S.E. (1978) Aminoglycoside antibiotics and eukaryotic protein synthesis: stimulation of errors in the translation of natural messengers in extracts of cultured human cells. *Biochemistry* **17**, 1149–1153
12. Lai, C.H., Chun, H.H., Nahas, S.A., Mitui, M., Gamo, K.M, Du, L., and Gatti, R.A. (2004) Correction of ATM gene function by aminoglycoside-induced read-through of premature termination codons. *Proc. Natl Acad. Sci. USA* **101**, 15676–15681
13. Schulz, A., Sangkuhl, K., Lennert, T., Wigger, M., Price, D.A., Nuuja, A., Gruters, A., Schultz, G., and Schoneberg, T. (2002) Aminoglycoside pretreatment partially restores the function of truncated V(2) vasopressin receptors found in patients with nephrogenic diabetes insipidus. *J. Clin. Endocrinol. Metab.* **87**, 5247–5257
14. Xi, B., Guan, F., and Lawrence, D.S. (2004) Enhanced production of functional proteins from defective genes. *J. Am. Chem. Soc.* **126**, 5660–5661
15. Barton-Davis, E.R., Cordier, L., Shoutourma, D.I., Leland, S.E., and Sweeney, H.L. (1999) Aminoglycoside antibiotics restore dystrophin function to skeletal muscles of *mdx* mice. *J. Clin. Invest.* **104**, 375–381
16. Politano, L., Nigro, G., Nigro, V., Piluso, G., Papparella, S., Paciello, O., and Comi, L.I. (2003) Gentamicin administration in Duchenne patients with premature stop codon. Preliminary results. *Acta Myol.* **22**, 15–21
17. Wilschanski, M., Yahav, Y., Yaacov, Y., Blau, H., Bentur, L., Rivlin, J., Avram, M., Bdolah-Abram, T., Bebok, Z., Shushi, L., Kerem, B., and Kerem, E. (2003) Gentamicin-induced correction of CFTR function in patients with Cystic Fibrosis and CTFR stop mutations. *N. Engl. J. Med.* **349**, 1433–1441
18. Thong, H.Y., Zhai, H., and Maibach, H.I. (2007) Percutaneous penetration enhancers: an overview. *Skin Pharmacol. Physiol.* **20**, 272–282
19. Kawamoto, T. (2003) Use of a new adhesive film for the preparation of multi-purpose fresh-frozen sections from hard tissues, whole-animals, insects and plants. *Arch. Histol. Cytol.* **66**, 123–143
20. Howard, M.T., Shirts, B.H., Petros, L.M., Flamigan, K.M., Gesteland, R.F., and Atkins, J.F. (2000) Sequence specificity of aminoglycoside-induced stop codon readthrough: potential implications for treatment of Duchenne muscular dystrophy. *Ann. Neurol.* **48**, 164–169
21. Auld, D.S., Thorne, N., Maguire, W.F., and Inglese, J. (2009) Mechanism of PTC124 activity in cell-based luciferase assays of nonsense codon suppression. *Proc. Natl Acad. Sci. USA* **106**, 3585–3590
22. Balfour, J.A. and Heel, R.C. (1990) Transdermal estradiol. A review of its pharmacodynamic and pharmacokinetic properties, and therapeutic efficacy in the treatment of menopausal complaints. *Drugs* **40**, 561–582
23. Marjukka Suhonen, T., Bouwstra, J.A., and Urtti, A. (1999) Chemical enhancement of percutaneous absorption in relation to stratum corneum structural alterations. *J. Control Release* **59**, 149–161
24. Cevc, G. (2003) Transdermal drug delivery of insulin with ultradeformable carriers. *Clin. Pharmacokinet.* **42**, 461–474
25. Roy, S. (1999) Preformulation aspects of transdermal drug delivery systems in *Transdermal and Topical Drug Delivery Systems* (Ghosh, T., Pfister, W., and Yum, S., eds), pp. 139–166, Interpharm, Buffalo Drove, IL
26. Wester, R. and Maibach, H. (1992) Percutaneous absorption of drugs. *Clin. Pharmacokinet.* **23**, 235–266
27. Williams, A.C. and Barry, B.W. (2004) Penetration enhancers. *Adv. Drug Deliv. Rev.* **56**, 603–618
28. Andersen, K.E., Maibach, H.I., and Anjo, M.D. (1980) The guinea-pig: an animal model for human skin absorption of hydrocortisone, testosterone and benzoic acid. *Br. J. Dermatol.* **102**, 447–453
29. Kushida, K., Masaki, K., Matsumura, M., Ohshima, T., Yoshikawa, H., Takada, K., and Muranishi, S. (1984)

Application of calcium thioglycolate to improve transdermal delivery of theophylline in rats. *Chem. Pharm. Bull.* **32**, 268–274
30. Zakzewski, C., Wasilewski, J., Cawley, P., and Ford, W. (1998) Transdermal delivery of regular insulin to chronic diabetic rats: effect of skin preparation and electrical enhancement. *J. Control Release* **50**, 267–272
31. Kanikkannan, N., Singh, J., and Ramarao, P. (1999) Transdermal iontophoretic delivery of bovine insulin and monomeric human insulin analogue. *J. Control Release* **59**, 99–105
32. Rastogi, S. and Singh, J. (2003) Passive and iontophoretic transport enhancement of insulin through porcine epidermis by depilatories: permeability and fourier transform infrared spectroscopy studies. *AAPS PharmSciTech* **4**, E29
33. Rastogi, S. and Singh, J. (2004) Iontophoretic enhancement of leuprolide acetate by fatty acids, limonene, and depilatory lotions through porcine epidermis. *Pharm. Dev. Tech.* **9**, 341–348
34. Lee, J.-N., Jee, S.-H., Chan, C.-C., Lo, W., Dong, C.-Y., and Lin, S.-J. (2008) The effects of depilatory agents as penetration enhancers on human stratum corneum structures. *J. Invest. Dermatol.* **128**, 2240–2247
35. Simon, G.A. and Maibach, H.I. (1998) Relevance of hairless mouse as an experimental model of percutaneous penetration in man. *Skin Pharmacol. Appl. Skin Physiol.* **11**, 80–86
36. Arakawa, M., Shiozuka, M., Nakayama, Y., Hara, T., Hamada, M., Kondo, S., Ikeda, D., Takahashi, Y., Sawa, R., Nonomura, Y., Sheykholeslami, K., Kondo, K., Kaga, K., Kitamura, T., Suzuki-Miyagoe, Y., Takeda, S., and Matsuda, R. (2003) Negamycin restores dystrophin expression in skeletal and cardiac muscles of *mdx* mice. *J. Biochem.* **134**, 751–758
37. Allamand, V., Bidou, L., Arakawa, M., Floquet, C., Shiozuka, M., Paturneau-Jouas, M., Gartioux, C., Butler-Browne, G., Mouly, V., Rousset, J.P., Matsuda, R., Ikeda, D., and Guicheney, P. (2008) Drug induced readthrough of premature stop codons leads to the stabilization of laminin alpha2 chain mRNA in CMD myotubes. *J. Gene Med.* **10**, 217–224
38. Hayashi, Y., Regnier, T., Nishiguchi, S., Sydnes, M.O., Hashimoto, D., Hasegawa, J., Kato, T., Kajimoto, T., Shiozuka, M., Matsuda, R., Noda, M., and Kiso, Y. (2008) Efficient total synthesis of (+)−Negamycin, a potential chemotherapeutic agent for genetic diseases. *Chem. Comm.* **20**, 2379–2381
39. Welch, E.M., Barton, E.R., Zhuo, J., Tomizawa, Y., Friesen, W.J., Trifillis, P., Paushkin, S., Patel, M., Trotta, C.R., Hwang, S., Wilde, R.G., Karp, G., Takasugi, J., Chen, G., Jones, S., Ren, H., Moon, Y.C., Corson, D., Turpoff, A.A., Campbell, J.A., Conn, M.M., Khan, A., Almstead, N.G., Hedrick, J., Mollin, A., Risher, N., Weetall, M., Yeh, S., Branstrom, A.A., Colacino, J.M., Babiak, J., Ju, W.D., Hirawat, S., Northcutt, V.J., Miller, L.L., Spatrick, P., He, F., Kawana, M., Feng, H., Jacobson, A., Peltz, S.W., and Sweeney, H.L. (2007) PTC124 targets genetic disorders caused by nonsense mutations. *Nature* **447**, 87–91

CELL STRUCTURE AND FUNCTION 34: 77–88 (2009)


# Ectopic Calcification is Caused by Elevated Levels of Serum Inorganic Phosphate in Mdx Mice

**Namiko Kikkawa[1], Tomohisa Ohno[1], Yosuke Nagata[1], Masataka Shiozuka[1], Toshihiro Kogure[2], and Ryoichi Matsuda[1]***

[1]*Graduate School of Arts and Sciences, The University of Tokyo, 3-8-1 Komaba, Meguro-ku, Tokyo 153-8902, Japan and* [2]*Department of Earth and Planetary Science, Graduate School of Science, The University of Tokyo, 7-3-1 Hongo, Bunkyo-ku, Tokyo 113-0033, Japan*

*ABSTRACT.* **Ectopic calcification occurs in the skeletal muscle of mdx mice, a dystrophin-deficient animal model of Duchenne muscular dystrophy. The purpose of this study was to clarify the mechanism of the calcification. The calcified deposits were identified as hydroxyapatite, a crystallized form of calcium phosphate, and the serum inorganic phosphate (Pi) level in the mdx mice was approximately 1.4 times higher than that in the normal B10 mice, suggesting that Pi plays a critical role in the ectopic calcification. When C2C12 mouse myoblasts were cultured under high-Pi conditions, myogenic differentiation was retarded while the expression of osteogenic markers such as osteocalcin and Runx2 were upregulated. This was followed by the generation of calcium deposition. Moreover, ectopic calcification reduced to an undetectable level in most of the mdx mice fed a Pi-reduced diet. We therefore conclude that the Pi-induced osteogenesis of muscle cells is responsible for ectopic calcification in the skeletal muscle of mdx mice.**

**Key words:** ectopic calcification/inorganic phosphate/mdx mouse/muscular dystrophy/skeletal muscle

## *Introduction*

Duchenne muscular dystrophy (DMD) is a progressive and genetic muscle disorder which leads to cardiac or respiratory failure resulting in the death of affected individuals by their late 20 s. DMD is caused by mutations in the dystrophin gene (Hoffman *et al.*, 1987). Dystrophin is the central component of the dystrophin-associated protein complex (DPC), which stabilizes the sarcolemma by forming a link between the actin cytoskeleton and laminin, an extracellular matrix protein (Ervasti *et al.*, 1990; Blake *et al.*, 2002). In the skeletal muscle of DMD patients and mdx mice, the animal model of DMD (Bulfield *et al.*, 1984), dystrophin is virtually absent. Dystrophin deficiency increases membrane fragility, which renders muscle fibers susceptible to damage during contraction (Petrof *et al.*, 1993, Matsuda *et al.*, 1995).

Ectopic calcification has been reported in various soft tissues such as the skin, kidney, tendons and blood vessels under pathological conditions (Giachelli, 1999). Calcification of the skeletal muscles in mdx mice and dystrophic dogs has also been reported (Geissinger *et al.*, 1990; Nguyen *et al.*, 2002), although its mechanisms remain entirely unclear. Calcification of cardiovascular tissue has been especially well studied for its clinical consequences, as vascular calcification in dialysis patients is associated with morbidity and mortality (Ketteler *et al.*, 2005). The inappropriate biomineralization of blood vessels had been regarded as a passive process caused by calcium phosphate precipitation (Schinke and Karsenty, 2000). However, within the last decade it has been suggested that vascular calcification is actively regulated by osteogenic gene expression in vascular smooth muscle cells (Giachelli, 1999). Attention has been focused on inorganic phosphate (Pi) as one of the factors regulating the observed cellular phenotypic changes, as cells cultured under high-Pi conditions undergo osteogene-

*To whom correspondence should be addressed: Ryoichi Matsuda, University of Tokyo, Room 309A, Building 15, 3-8-1 Komaba, Meguro-ku, Tokyo 153-8902, Japan.
Tel: +81–3–5454–6637, Fax: +81–3–5454–4306
E-mail: cmatsuda@mail.ecc.u-tokyo.ac.jp

Abbreviations: 3-D: 3-dimensional; BMP-2: bone morphogenetic protein-2; CT: computed tomography; DMD: Duchenne muscular dystrophy; DMEM: Dulbecco's modified Eagle's medium; DPC: dystrophin-associated protein complex; GAPDH: glyceraldehyde-3-phosphate; EDS: energy-dispersive X-ray spectrometry; FGF-23: fibroblast growth factor-23; HA: hydroxyapatite; MyHC: myosin heavy chain; PBS: phosphate buffered saline; Pi: inorganic phosphate; SEM: scanning electron microscopy; TEM: transmission electron microscopy

sis and form calcium depositions *in vitro* (Jono *et al.*, 2000).

The main objective of this study was to uncover the nature of calcification in mdx mouse skeletal muscle. Since muscle satellite cells possess multilineage potential (Asakura *et al.*, 2001; Wada *et al.*, 2002), we tested the hypothesis that the osteogenesis of muscle cells is the key cause of ectopic calcification in mdx mice.

## Materials and Methods

### Animal care and dietary treatment

Mdx and normal C57BL/10 mice, provided by the National Center of Neurology and Psychiatry (Japan), were kept at 25°C under a 12 h light-dark cycle in a conventional animal-care facility. A low Pi diet (0.1% Pi instead of 0.9% Pi in normal diet) was manufactured by Oriental Yeast (Tokyo, Japan). For Pi uptake restriction, the mice were fed the low Pi diet during lactation and after weaning until reaching 2 months of age. The animals were euthanized with an overdose of ether gas. The animal experiments were carried out according to the animal experimental manual of the University of Tokyo.

### Antibodies

The primary antibodies used were as follows: anti-sarcomeric myosin heavy chain (MyHC) mouse monoclonal antibody MF20 (Developmental Studies Hybridoma Bank, University of Iowa, Iowa City, Iowa), mouse monoclonal anti-myogenin antibody F5D (Developmental Studies Hybridoma Bank), rabbit polyclonal anti-Runx2 (transcription factor expressed during osteogenesis) antibody (Santa Cruz Biotechnology, Santa Cruz, CA) and rat polyclonal anti-F4/80 (glycoprotein expressed by mature macrophages) antibody (Serotec, Oxford, UK). The secondary antibodies used for immunohistochemistry were Alexa Fluor 488-conjugated goat anti-mouse IgG, Alexa Fluor 488-conjugated goat anti-rat IgG and Alexa Fluor 594-conjugated goat anti-rabbit IgG (Invitrogen, Carlsbad, CA); those for Western blotting were IRDye 800-conjugated goat anti-mouse IgG (Rockland, Gilbertsville, PA) and Alexa Fluor 680-conjugated goat anti-rabbit IgG (Invitrogen). All diluted antibodies were centrifuged at 15,000×*g* for 5 min prior to use in order to eliminate aggregates.

### X-ray micro CT observation

The lower limbs of mdx and B10 mice were excised and wrapped in NOVIX parafilm (AGC Techno Glass, Chiba, Japan), mounted on the stage with plasticine, and scanned using the high-resolution X-ray micro-computed tomography (CT) SkyScan-1074 scanner (SkyScan, Kontich, Belgium) operated at 40 kV and 1000 μA. X-ray transmission images were acquired from a longitudinal view rotated every 0.9-degrees under a 660-msec exposure. CT images at a resolution of 22 μm were reconstructed using cone-beam reconstruction software (SkyScan) before 3-dimensional (3-D) images were generated with the image analysis software CTAn (SkyScan). Calcification was quantified using the 3-D analysis software CT Vol (SkyScan). After the CT analysis, calcified areas of mdx mice were fixed with 10% formalin in phosphate buffered saline (PBS) for further X-ray analysis or embedded in OCT compound (Sakura Finetechnical, Tokyo, Japan) before being frozen in liquid nitrogen-cooled melting isopentane. Transversal cryosections with 5 μm thickness were prepared for von Kossa, alizarin red S and immunofluorescent stainings. Von Kossa stained samples were counterstained with nuclear fast red. For whole-body imaging, mdx mice were deeply anesthetized by an intraperitoneal injection of pentobarbital (50 mg/kg body weight, Dainippon Sumitomo Pharma, Osaka, Japan) and subjected to X-ray micro CT scanning on a LaTheta LTC-100 (Aloka, Tokyo, Japan).

### Scanning Electron Microscopy (SEM) and Transmission Electron Microscopy (TEM) analyses

Muscle calcification was identified by back-scattered electron imaging and energy-dispersive X-ray spectrometry (EDS) analysis of a piece of dried muscle coated with a thin carbon film using a S-4500 SEM (Hitachi, Tokyo, Japan) operated at 15 kV. The piece of muscle was also ground and suspended in ethanol, then dispersed on a holey carbon microgrid (Nissin EM, Tokyo, Japan) for TEM investigation. A JEM-2010 TEM (JEOL, Tokyo, Japan) equipped with an EDS detector was used to identify the mineral phase by analyzing the composition and electron diffraction pattern of the sample.

### Measurements for Serum calcium, Inorganic Phosphate (Pi), and Fibroblast Growth Factor (FGF)-23

Mouse blood was collected via a retro-orbital sinus puncture and incubated overnight at 4°C. Serum was subjected to calcium and Pi measurements using the automated clinical chemistry analyzer Fuji Dri-chem 4000 (Fujifilm, Tokyo, Japan) based on colometric analysis using the chlorophosphonazo-III and purine nucleoside phosphorylase reactivity, respectively (Ferguson *et al.*, 1964; Hwang *et al.*, 1973). For FGF-23 measurements, mouse sera collected as described above were tested for FGF-23 concentration using an FGF-23 ELISA kit (Kainos Laboratories, Tokyo, Japan).

### Cell cultures

C2C12 mouse myoblasts were cultured in a growth medium (high-glucose Dulbecco's modified Eagle's medium (DMEM: Gibco, Grand Island, NY) containing 20% fetal bovine serum (JRH Biosciences, Lenexa, KS), 50 IU/ml penicillin, and 50 μg/ml streptomycin (Gibco)). The cells were trypsinized before reaching confluency and reseeded at an initial density of $1\times10^4$ cells/cm$^2$ in gelatin-coated Petri dishes (AGC Techno Glass, Chiba, Japan). After 24 h incubation, the growth medium was replaced with differentiation medium (DMEM containing 2% horse serum (Gibco) and penicillin-streptomycin). For the primary culture, cells were prepared from the mdx mouse rectus femoris muscle by 0.5%

trypsin digestion, resuspended in primary culture medium (DMEM containing 20% fetal bovine serum, 10% horse serum and penicillin-streptomycin) and then seeded in gelatin-coated Petri dishes. The differentiation medium and the primary culture medium contained 1.0 mM and 1.3 mM of Pi, respectively. For the induction of calcification, the media were supplemented with Pi solution (NaH2PO4-Na2HPO4, pH 7.4) to a final concentration of 3~9 mM. Likewise, 5 mM of Pi and 2 mM of calcium chloride were added to the differentiation medium to enhance calcium phosphate deposition. The cells were cultured at 37°C and 5% $CO_2$ in a humidified atmosphere.

### *Quantification of calcium deposition*

C2C12 cells seeded in 24-well plates (AGC Techno Glass) were cultured as described above. After fixation with 10% formalin in PBS for 30 min at room temperature, the cells were washed 3 times in PBS and treated with a 2N HCl solution overnight at room temperature to dissolve the calcium depositions. The calcium concentration of the supernatant was measured using the Calcium E-test (Wako Pure Chemical Industries, Osaka, Japan) based on the *o*-cresolphthalein complexone method (Gindler and King, 1972). After the calcium measurement, the cells were washed 3 times in PBS, lysed in 125 mM Tris-HCl (pH 6.8) with 2% SDS for 10 min on ice, and the protein concentration of the supernatant was then determined using BCA Protein Assay Reagent (Pierce, Rockford, IL). The absorption at 595 nm was observed on a Model 680 Microplate Reader (Bio-Rad, Hercules, CA) for both assays. The calcium content was normalized to the total protein content in each well.

### *Immunofluorescent staining*

Muscle tissue cryosections 5 μm in thickness were fixed with 10% formalin in PBS for 30 min at room temperature. The cultured cells were subjected to the same procedure, but were treated with 0.5% Triton X-100 (ICN Biochemicals, Aurora, OH) in PBS to permeabilize the cell membrane before incubation with the primary antibody. The samples were reacted with the primary antibody overnight, followed by washing 3 times in PBS. The secondary antibody was applied to the section for 1 h at room temperature and washed again 3 times in PBS. Five μg/ml of Hoechst 33258 (Sigma Aldrich, St. Louis, MO) was added to the secondary antibody solution to visualize the nuclei. For the negative controls, the primary antibody was replaced with PBS. All antibodies were appropriately diluted in PBS containing 0.5% bovine serum albumin (Sigma Aldrich).

The fusion index, defined as the ratio of the nuclei in multinuclear myotubes to all the nuclei, was used as a marker of muscle differentiation. More than 600 nuclei were counted for each sample.

### *Western blot analysis*

C2C12 cells were fixed with 10% trichloroacetic acid (Wako Pure Chemical Industries) in PBS for 30 min at 4°C, rinsed 3 times with ice-cold PBS, scraped off the plate, and then collected by centrifugation at 15,000×*g* for 5 min. The pellets were lysed by sonication in sample buffer (125 mM Tris-HCl and 2% SDS, pH adjusted to 6.8). The total protein concentration of the lysates was determined using BCA Protein Assay Reagent (Pierce, Rockford, IL) and adjusted to an equal concentration before boiling for 5 min in the presence of 0.1 M DTT (Wako Pure Chemical Industries). The proteins were subjected to 18% SDS-PAGE and transferred to an Immobilon-FL PVDF membrane (Millipore, Billerica, MA). After incubating in Odyssey Blocking Buffer (LI-COR Biosciences, Lincoln, NE) for 2 to 4 h, the membranes were probed with primary antibody overnight at room temperature. The membranes were washed 3 times in PBS containing 0.5% Tween 20 (ICN Biochemicals), followed by a 1 h incubation with the secondary antibody, and again washed 3 times in PBS/Tween 20. All antibodies were diluted in Odyssey Blocking Buffer. The protein bands were visualized using the Odyssey Infrared Imaging System (LI-COR Biosciences) which allows multiplex detection; thus, an objective protein and an internal loading control can be detected on the same membrane at the same time.

### *RT-PCR*

RNA samples were collected from C2C12 cells using RNA-Bee (IsoTex Diagnostics, Friendswood, TX) and reverse transcription was performed using the First Strand cDNA Synthesis Kit (Marligen Biosciences, Ijamsville, MD) according to manufacturers' protocols. PCR amplification was carried out with Premix Taq (Takara Bio Inc, Shiga, Japan). Primer sequences of osteocalcin (forward: 5'-CAA GTC CCA CAC AGC AGC TT-3', reverse: 5'-AAA GCC GAG CTG CCA GAG TT-3') and glyceraldehyde-3-phosphate (GAPDH, forward: 5'-GTG AAG GTC GGA GTC AAC G-3', reverse: 5'-GGT GAA GAC GCC AGT GGA CTC-3') were obtained from previous studies (Desbois *et al.*, 1994; Ploszaj *et al.*, 1998).

## *Results*

### *X-ray micro CT observation*

The hind limbs of mdx and B10 mice at various ages were scanned with an X-ray micro CT scanner (Fig. 1). Fig. 1A shows representative images of the hind limb from a 2-month-old mdx mouse. The bony structure in the middle of the X-ray transmission image is the femur. X-ray-absorbing particles aligned towards the direction of muscle fibers were found in the skeletal muscle tissues by CT (Fig. 1A-CT), but were barely observable in the X-ray transmission image. Ninety-two percent of mdx mice exhibited these particles (N=12), while no such structures were observed in B10 mice (Fig. 1B, N=8). The particles found in the mdx mice were also detectable non-invasively using the whole-body X-ray micro CT scanner LaTheta LTC-100 (Fig. 1C).

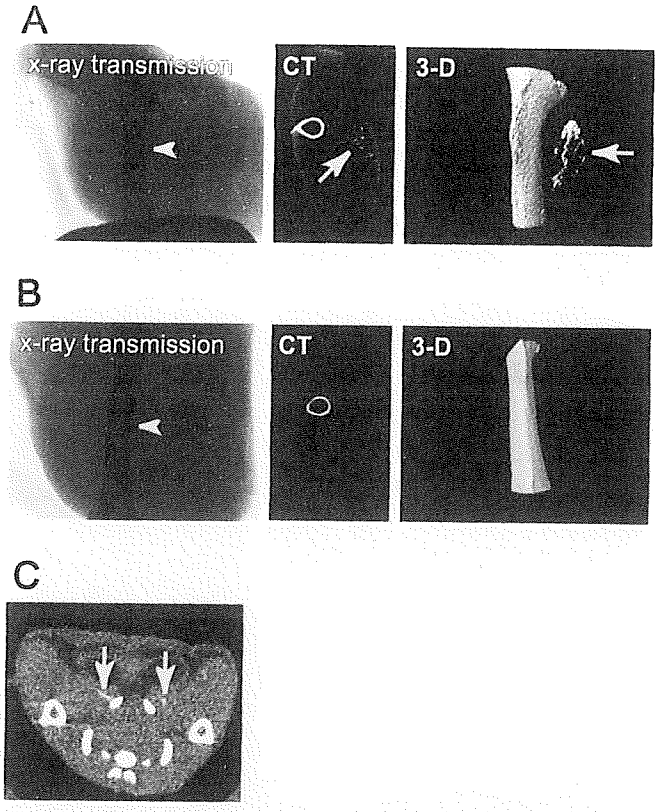


**Fig. 1.** (A) Images of the hind limb of a 2-month-old mdx mouse, obtained using the X-ray micro CT scanner SkyScan 1074. X-ray transmission image: X-ray-absorbing materials are shown as gray shadows, and the femur (indicated by the arrowhead) can be seen in the middle of the X-ray. CT image: the grayscale was inverted, and the X-ray-absorbing substances are shown in white. The white loop in the middle signifies the femur. X-ray-absorbing particles (indicated by the arrow) apparently differing from bone can be observed. Reconstructed 3-D image: X-ray-absorbing particles (indicated by the arrow) are distributed parallel to the femur in skeletal muscle tissue of the mdx mouse. (B) Images of the hind limb of a 2-month-old B10 mouse obtained using the X-ray micro CT scanner SkyScan 1074. The femur is indicated by the arrowhead. No calcification was observed in the X-ray transmission, CT and 3-D images. (C) A CT image of the lower abdomen of a mdx mouse obtained using the whole-body X-ray micro CT scanner LaTheta LTC-100. The X-ray-absorbing particles are indicated by arrows.

### *Identification of the mineral phase by SEM and TEM*

Fig. 2A shows a back-scattered electron image obtained by SEM from a cross-section of the muscle from the hind-limb of an mdx mouse. Some muscle bundles displayed a bright contrast, corresponding to a large atomic number. The EDS spectra obtained from these brightly-contrasted bundles indicated the presence of both calcium and phosphorus, which suggested the formation of a calcium phosphate phase (data not shown). To determine the mineral phase, the specimen was further analyzed using TEM. Fig. 2B is a TEM image of the calcium-containing material, and the electron diffraction pattern from the material within the white circle in Fig. 2B is shown in Fig. 2C (top-left and bottom-right). A simulation of the diffraction pattern (Fig. 1C, top-right and bottom-left) using the crystallographic parameters of hydroxyapatite (HA, Ca5(PO4)3OH) showed an almost identical match between the observed and simulated electron diffraction patterns. This indicates that the observed calcification of the muscle was due to a precipitation of HA particles. The EDS spectrum (Fig. 2D) taken from the sample within the white circle in Fig. 2B also confirmed the presence of calcium and phosphorus, providing strong evidence that the material was indeed HA. Therefore, these particles are hereafter referred to as "ectopic calcification."

### *Histological staining*

A cryosection of 2-month-old mdx mouse skeletal muscle was von Kossa-stained to confirm the presence of calcium (Fig. 3A). von Kossa-positive particles were observed, suggesting that they consisted of calcium. Other cryosections were stained with alizarin red S or antibodies for F4/80 (Fig. 3B). The calcified areas stained dark red (Fig. 3B-a) and the serial section, washed gently under running water beforehand, was also positively-stained (Fig. 3B-b). Some of the muscle fibers were alizarin red S-positive when stained without the pre-washing procedure (Fig. 3B-d); however, after washing they turned negative (Fig. 3B-e). We presumed that in these particular fibers, calcium ions had accumulated prior to calcium deposition in the form of HA particles.

Another set of serial sections were immunostained for F4/80, a transmembrane protein expressed in macrophages and widely used as a macrophage marker. Macrophage accumulation was observed in the areas surrounding calcification (Fig. 3B-c) and in calcium-rich muscle fibers (Fig. 3B-f). No alizarin red S-positive fibers were observed in the B10 mice before (Fig. 3B-g) or after washing (Fig. 3B-h). Macrophage accumulation (Fig. 3B-i) was not detected in the B10 mice.

### *Serum Calcium, Pi, and FGF-23 measurement*

As we confirmed that ectopic calcification is composed of HA, a major form of calcium phosphate in vertebrates, a metabolic disorder of calcium or phosphate was suspected in the mdx mice. The serum Pi and calcium levels in mdx and B10 mice at 2 months of age were compared (Fig. 4). While no significant difference in serum calcium was observed between the B10 and mdx mice, the serum Pi level of the mdx mice was significantly higher compared to that of the B10 mice. These results were consistent with a previous study by Brazeau *et al.* (1992). The serum level of FGF-23, a protein which regulates serum phosphate level by suppressing renal Pi absorption, was also measured in the

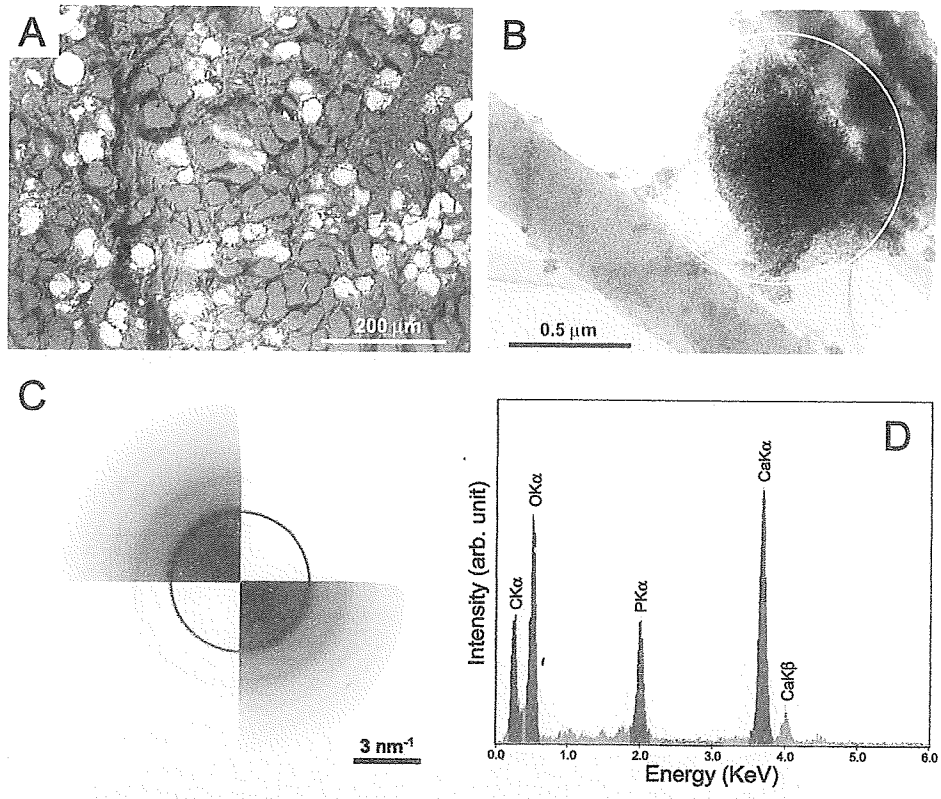


**Fig. 2.** (A) Back-scattered SEM image from a cross-section of mdx skeletal muscle. The calcified muscle bundles are shown in bright contrast. (B) TEM image of ground mdx skeletal muscle. Inorganic material can be observed between the muscle fibers. (C) Electron diffraction pattern (top-left and bottom-right) from within the white circle in (B) and the simulated pattern for hydroxyapatite (HA) (top-right and bottom-left). (D) EDS spectrum obtained from the material within the white circle in (B).

2-month-old B10 and mdx mice. The serum FGF-23 concentration of mdx mice was significantly higher than in the B10 mice (Fig. 4).

### *Detection of Pi-induced osteogenesis in C2C12 cells*

To study the effects of Pi in muscle cell differentiation, murine myoblast-derived C2C12 cells were cultured for 4 days under various Pi concentrations and immunostained for the presence of myogenic and osteogenic markers (Fig. 5A–C). The cells underwent muscle differentiation and formed myotubes when cultured in normal differentiation medium (Pi=1 mM). Myogenesis proceeded until the Pi concentration of the differentiation medium reached 5 mM, but myotube formation was strongly suppressed at 7 mM (Fig. 5A). The retardation of myogenesis caused by the high Pi concentration was also evident by the decrease in the fusion index and myogenin expression (Fig. 5B). The expressions of Runx2, a transcription factor of osteogenesis and used as an osteogenic marker, increased with the rise of the Pi concentration (Fig. 5B). It is notable that under the condition of 5 mM Pi, myogenesis was not inhibited and the cells differentiated into myotubes, while the expression of Runx2 was augmented. Further observation revealed that myogenin and Runx2 did not colocalize in the same nuclei. Runx2 expression in the myotubes was observed not in the nuclei, but in the cytoplasm (Fig. 5C). This suggests that Runx2 is inactive in myogenic cells, as it has been reported that Runx2 activity is regulated by translocation between the nucleus and the cytoplasm (Zaidi *et al.*, 2001).

Likewise, upregulation of Runx2 expression was observed by Western blotting not only when the cells were cultured under high-Pi conditions, but also when cultured in the presence of calcium phosphate deposits, which were generated by the addition of sodium phosphate and calcium chloride to the medium (Fig. 5D).

To study the expression of osteocalcin, a secreted protein whose expression is regulated by Runx2 (Xiao *et al.*, 1999) and used as another marker for osteogenesis, RT-PCR was performed with RNA samples prepared from C2C12 cells cultured under various Pi concentrations for 4 days. Osteocalcin expression was undetectable when the cells were cultured with 1 mM Pi, but increased with the elevation of the Pi concentration (Fig. 5E).

The calcium deposition in C2C12 cells cultured under various Pi concentrations was measured and normalized to

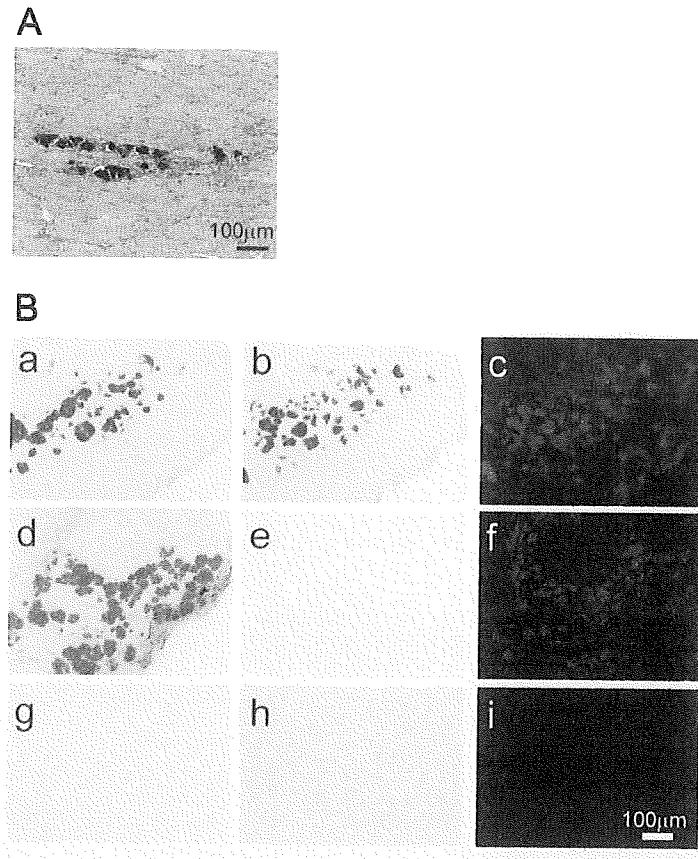


**Fig. 3.** Von Kossa, alizarin red S-stained and immunostained cryosections of mdx and B10 mice skeletal muscle. (A) Von Kossa-stained section of a 2-month-old mdx mouse hind limb. The X-ray-absorbing particles detected by the X-ray micro CT scanner are stained black. (B-a, d) Alizarin red S-stained cryosections of mdx mouse skeletal muscle. The calcified or calcium-rich areas are stained red. (B-b, e) Serial sections of (B-a) and (B-d) stained with alizarin red S after washing with tap water. The calcified areas were stained red (B-a), and remained alizarin red S-positive after washing (B-b). There were some muscle fibers which were alizarin red S-positive before washing (B-d), but turned negative after washing (B-e). These fibers are presumed to contain high concentrations of calcium ions and are undergoing calcification. (B-c, f) Another set of serial sections of (B-a) and (B-d) were immunostained for F4/80. Macrophages are accumulated in both regions. (B-g, h) Alizarin red S-stained cryosections from a B10 mouse before (B-g) or after (B-h) washing. No positive fibers were observed. (B-i) Serial section of (B-g) immunostained for F4/80. No macrophage accumulation was observed.

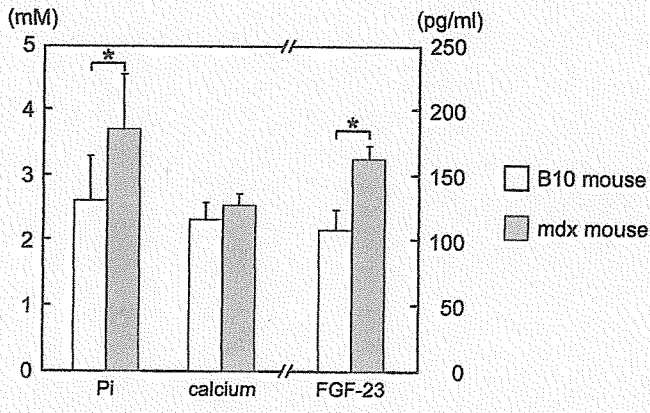


**Fig. 4.** Serum Pi and calcium levels of B10 and mdx mice at 2 months of age. The serum Pi concentration of mdx mice was 1.41 times higher than in B10 mice, while no significant difference was observed in the calcium concentration between the 2 strains. The serum FGF-23 concentration of mdx mice was 1.5 times higher than in B10 mice. (*: $p<0.05$)

the corresponding protein content at day 7 (Fig. 6). The cells did not deposit calcium under normal Pi conditions, whereas the cells cultured in medium containing 3 mM of Pi or higher deposited calcium. The amount of calcium increased significantly at higher Pi concentrations.

### *Pi-induced calcification in the primary culture of skeletal muscle cells*

Cells isolated from mdx skeletal muscle tissue were cultured in normal Pi (1.3 mM) or high-Pi (5 mM) medium to study the effects of Pi in primary culture cells (Fig. 7). The cells formed myotubes when cultured in normal medium, while myotube formation was strongly inhibited under high-Pi conditions. Both alizarin red S staining and von Kossa staining revealed that numerous calcium deposits were present after 10 days of culture in high-Pi medium, but were not detected in cells cultured in normal medium.

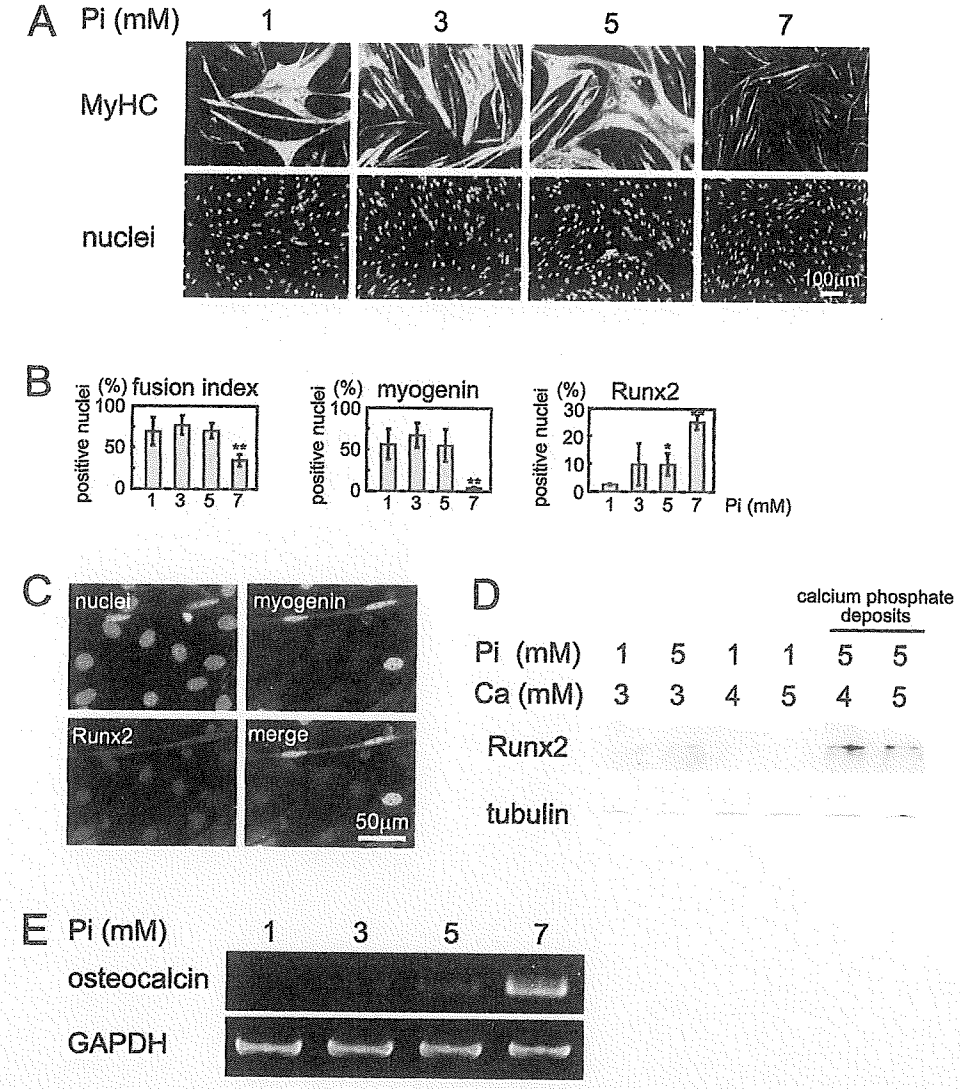


**Fig. 5.** Immunocytochemistry and RT-PCR of C2C12 cells cultured under various Pi concentrations. The Pi concentration of each condition was 1, 3, 5, and 7 mM. (A) Cells immunostained for MyHC (green). MyHC-positive myotubes formed at 1, 3 and 5 mM Pi but were completely absent at 7 mM. Nuclei were stained with Hoechst 33258 (blue). (B) The myogenin expression, the fusion index, and the expression of Runx2 were quantified. The fusion index and ratio of the nuclei expressing myogenin decreased, while the ratio of Runx2-expressing nuclei increased with increasing Pi concentration. (*: $p<0.05$; **: $p<0.01$). (C) Close observation of cells cultured in medium containing 5 mM of Pi, stained with Hoechst 33258 to show the nuclei or immunostained for myogenin or Runx2. The cells did not express myogenic and osteogenic markers at the same time. (D) Western blotting of C2C12 cells cultured under increased Pi or calcium concentrations. Runx2 expression was enhanced when the cells were co-cultured with calcium phosphate deposits. (E) RT-PCR for osteocalcin in C2C12 cells cultured in media containing 1, 3, 5, and 7 mM Pi. Osteocalcin mRNA was not detected at 1 mM Pi but increased with increasing Pi concentrations. GAPDH was used as an internal control.

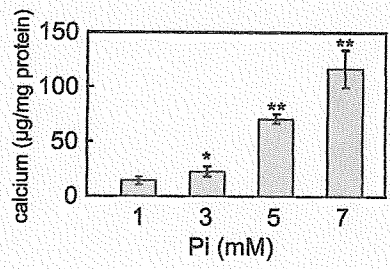


**Fig. 6.** Quantification of calcium deposits generated by C2C12 cells cultured under various Pi concentrations. Calcium deposition increased with increasing Pi concentrations. No calcification was observed in cells culture under normal conditions. (*: $p<0.05$, **: $p<0.01$.)

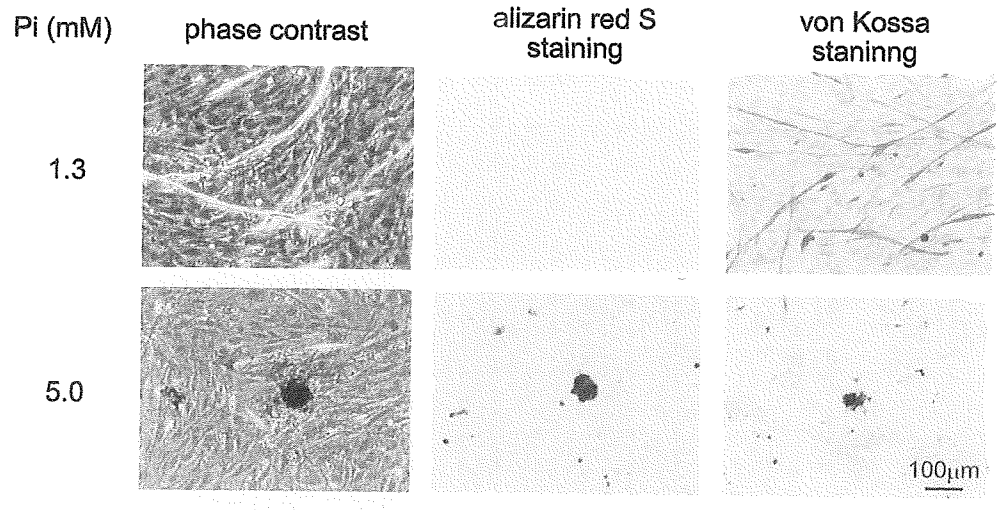


**Fig. 7.** Calcification of mdx mouse muscle-derived primary culture cells. Cells were cultured for 10 days at a Pi concentration of 1.3 mM or 5 mM. Calcium depositions were stained red or black with alizarin red S and von Kossa staining, respectively, while no calcification was observed when the cells were cultured in normal medium containing 1.3 mM of Pi. The von Kossa-stained samples were counterstained with nuclear fast red, and the myotubes were stained pink.

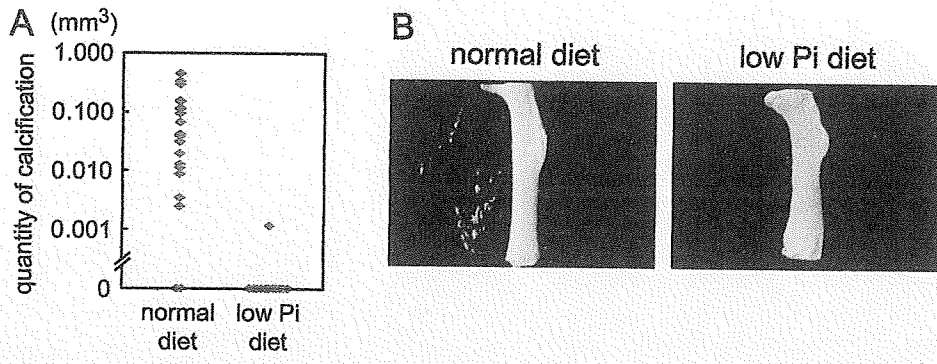


**Fig. 8.** Inhibition of ectopic calcification in mdx mice by a low Pi diet. (A) Quantity of ectopic calcification observed in mdx mice fed a normal or low Pi diet for 2 months. The mass of calcification per 1 hind limb significantly decreased when mice were fed the low Pi diet. (B) Reconstructed 3-D images of the hind limb of an mdx mouse fed a normal or low Pi diet. Ectopic calcification, which was observed in mdx mice fed the normal diet, disappeared in 83% of the hind limbs of mdx mice fed the low Pi diet.

### *Inhibition of ectopic calcification in mdx mouse skeletal muscle by a low Pi diet*

To investigate the role of Pi in ectopic calcification *in vivo*, mice were fed a low Pi diet for 2 months. Serum Pi level decreased in both B10 (1.6±0.13 mM) and mdx mice (2.1±0.51 mM), and the restriction of Pi intake seemed to correct serum Pi elevation in mdx mice. However, the serum calcium level was elevated in both B10 (3.5±0.25 mM) and mdx mice (3.0±0.08 mM).

A low Pi diet also inhibited ectopic calcification in mdx mouse skeletal muscle (Fig. 8). The quantity of ectopic calcification of 2-month-old B10 and mdx mice in each diet group (N=6) was determined. Fig. 8A shows the mass of calcification per one hind limb of the mdx mouse fed a normal or low Pi diet. Ectopic calcification was observed in all hind limbs of the mdx mice fed with normal diet. However, calcification was undetectable in 5 out of 6 (83%) of the mdx mice fed a low Pi diet (Fig. 8B), and one mouse showed small-scale calcification in one of the hind limbs, whose quantity was decreased 78-fold compared to the average of the mdx mice fed with normal diet. B10 mice exhibited no calcification in either diet groups. No significant difference was observed in the body weight or survival rate between both diet groups of the B10 or mdx mice (data not shown).